Silicon
https://doi.org/10.1007/s12633-020-00522-1

ORIGINAL PAPER

Ultra-High Capacity FSK Transmission Using Silicon Microring Embedded Gold Grating Circuits

A. E. Arumona [1,2,3] · I. S. Amiri [1,2] · S. Punthawanunt [4] · K. Ray [5] · P. Yupapin [1,2]

Received: 13 December 2019 / Accepted: 13 May 2020

Abstract

The Frequency Shift Keying (FSK) dual-transmission mode for short-range communication using the silicon microring resonator arrangement is proposed. FSK generated by an optical modified add-drop multiplexer embedded gold grating connected to three other microring resonators. The proposed system consists of a transmitted microring with two nano-ring phase modulators, which connected through a 10 km fiber channel to a receiver. The user end consists of three similar microring systems. A gold grating embedded on two side ring center (sensor probe) to introduce the plasmonic polariton, from which each of sensor probe identified by the Bragg wavelength. The frequency of n photonic oscillator is in the range of plasmonic frequencies, where the Whispering Gallery Mode (WGM) due to the light propagations can be obtained by controlling the used two sides smaller ring resonator in the proposed ring structures. The WGM beam can be used as another mode of transmission called light fidelity (LiFi) transmission. In manipulation, the FSK light source wavelength of 1.55 μm fed into the system. The transmission bit rates of 200 Tbits$s^{-1}$is achieved. The Bit Error Rate (BER) obtained at the user ends increases with increasing input power. Each sensor node identified the Bragg wavelength, while the change in Bragg wavelength on each sensor obtained and shown the linear trend, which is useful for sensing application. In applications, the proposed system is capable of dual mode of transmission either cable or wireless and in this case, the cable transmission of data using LiFi is more reliable than WiFi in terms of security, efficiency, availability, and safety.

Keyword Silicon microring · Gold grating · Microring circuit · FSK · THz frequency · LiFi

1 Introduction

FSK (frequency-shift keying) is frequency modulation, where data transmitted via discrete frequency changes of a carrier wave. FSK is the well-established technique in the twentieth century, where principally, it is implemented by making use of oscillators and the switching process that involves changing to a different frequency at the start of each symbol period [1].The noise against FSK is small and which makes FSK very robust. There are different types of FSK, for an instant, the binary FSK, which is a type modulation. It is a simple nonlinear form of FSK because BFSK transmits the binary forms (0 and 1) of discrete frequency. It is a pair of signals having the advantages in remote sensing and caller identification (ID) applications [2]. The others are CPFSK (continuous phase), GFSK (Gaussian), audio FSK, MSK (minimum), GMSK (Gaussian minimum), MFSK (multiple) and so much more [3]. The easy in implementing and decoding FSK makes the best choice in usage. It operates in almost any wires available that makes it useful in communication over a long distance. The well-known problem of FSK is that the bandwidth requirement is very high. LiFi (light fidelity) proposed by Harald

✉ P. Yupapin
preecha.yupapin@tdtu.edu.vn

A. E. Arumona
arumonaarumonaedward.st@student.tdtu

K. Ray
kray@jpr.amity.edu

[1] Computational Optics Research Group, Advanced Institute of Materials Science, Ton Duc Thang University, District 7, Ho Chi Minh City 700000, Vietnam

[2] Faculty of Applied Sciences, Ton Duc Thang University, District 7, Ho Chi Minh City 700000, Vietnam

[3] Division of Computational Physics, Institute for Computational Science, Ton Duc Thang University, Ho Chi Minh City 700000, Vietnam

[4] Faculty of Science and Technology, Kasem Bundit University, Bangkok 10250, Thailand

[5] Amity School of Applied Sciences, Amity University Rajasthan, Jaipur, India

Published online: 25 May 2020

[4] in which LiFi could replace WiFi. A LiFi frequency range has more than the WiFi range, where the available LiFi frequency range is 340 THz [5–8], while the WiFi frequency range is less than 1 GHz. The LiFi applications are ranging from the public internet via LED (light emitting diode) to cars and auto-piloted. It can be used in hospitals and aircraft, which has a problem with electromagnetic interference, and so much more. LiFi makes use of modulation in its operation; while changing the light intensity, LiFi's information can be varied [9–11]. LiFi can be differently implemented using microring resonator in which the concept of WGM is used and also embedding the microring with gold grating for LiFi-quantum [12–14]. Although despite the numerous advantage of LiFi over WiFi; LiFi is still in its early stage and a long way to go before becoming available commercially. Noel [15] implemented FSK using the LMX2571 device, in which frequency modulation and GFSK modulation used. Mahendra [16] implemented BFSK modulation and demodulation using HC/HCT4046A device. Todd [17] applied FSK modulation and demodulation using PSOC3 and PS0C5LP device. Hemalatha et al. [18] generated FSK using the software define ratio (SDR), which is the implementation of FSK transceiver using SDR. Wu [19] implemented FSK modulation using the FPGA (field programmable gates array).In this present work, the FSK implemented using the silicon microring circuit, which can apply in dual-LiFi-cable transmission modes. By using the graphical program, the required output obtained by using the suitable parameters. The parameters extracted from the Optiwave program will be used in the MATLAB program to find the bit error rate (BER) and change in Bragg wavelength with increasing input power. The applied sensor nodes can be identified, which are available for sensing applications. The sensing signals obtained by the plasmonic waves that propagated through the gold material, which applied for the electro-optic signal conversion. The related theory and further potential applications are given and discussed, respectively.

2 Background

The FSK advantage is that it has high immunity to noise, high signal to noise ratio, and high data rate compared to ASK (amplitude shift key) and PSK (phase shift key) but its drawback is larger bandwidth required. The FSK modulating signal is binary 1 or 0, which have two frequencies given by the general form as [19]:

$$\boldsymbol{FSK} = \boldsymbol{A}\exp\left[-2\pi \boldsymbol{i}\left(\sum_{i=1}^{n} \boldsymbol{f}_i \boldsymbol{t}_i\right)\right] \quad (1)$$

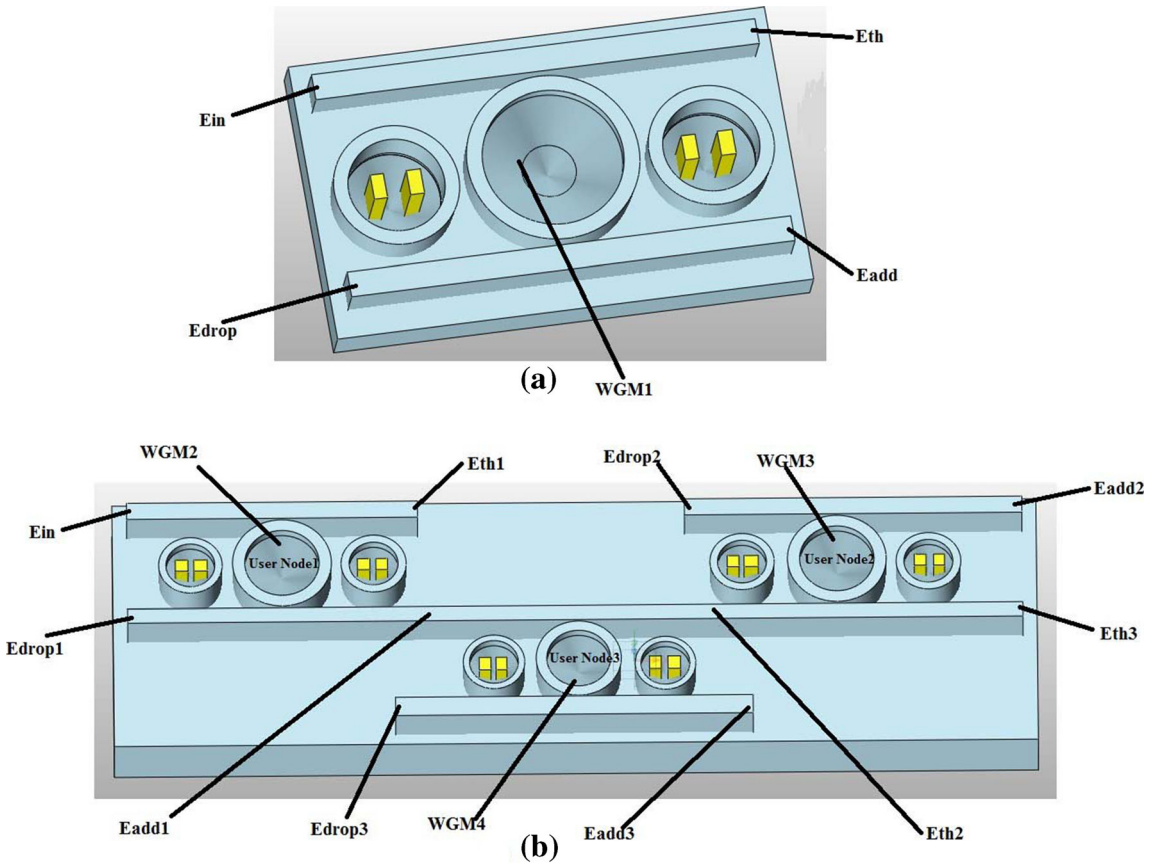

Fig. 1 A schematic of a circuit used in the simulation, where (a) the transmission circuit, (b) the distributed nodes, Ein: input port, Edrop: drop port, Eth: throughput port, Edd: add port

Table 1 The selected parameters of the system used in the simulation

Parameters	Values	Units
Input signal power (Gaussian pulse) (P)	1.0–10.0	mW
Si-linear waveguide length (L)	16.0	μm
Si center ring/radius (R)	3.0	μm
Si small ring/radius (R_1)	1.50	μm
Si small ring/radius (R_2)	1.50	μm
Gold/thickness (d)	0.10	μm
Gold/length (L)	0.50	μm
Gold dielectric constant (ϵ_o) [24] พิมพ์สมการที่นี่	6.90	
Gold permittivity (ϵ_o) [24]	10.0	
Coupling coefficient (κ)	0.50	
Refractive index Si (n_{Si}) [25]	3.42	
Gold refractive index (n_{Gold}) [25]	1.80	
Silicon nonlinear refractive index (n_2) [26]	1.3×10^{-13}	m^2W^{-1}
Input light wavelength (λ)	1.55	μm
Waveguide core effective area (A_{neff}) [27]	0.30	μm^2
Waveguide loss (α)	0.50	$dB.(mm)^{-1}$
Grating period (Λ)	0.50	μm
Fiber loss	0.10	$dBkm^{-1}$

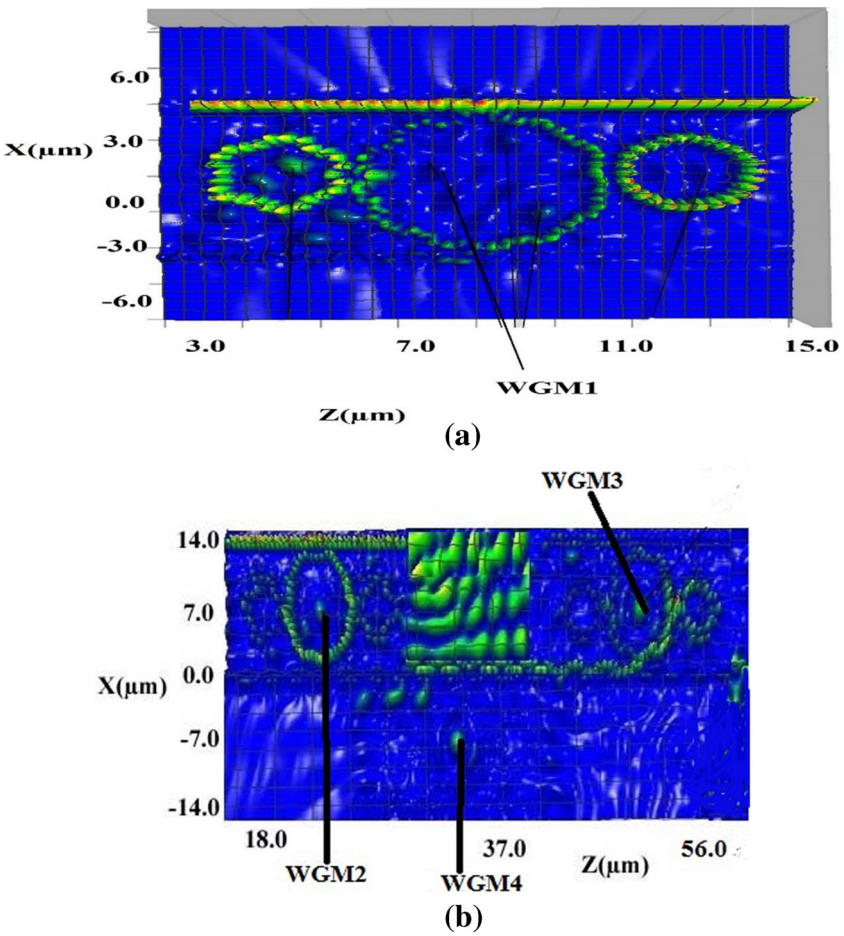

Fig. 2 The graphical results, where (a) input power = 10 mW, and (b) input power = 6.88 mW, where the used parameters are the center wavelength = 1.55 μm, $R_{Si} = 3$ μm, $R_1 = R_2 = 1.50$ μm, the other parameters are given in Table 1. WGM1-WGM4 are the whispering gallery modes at the center rings

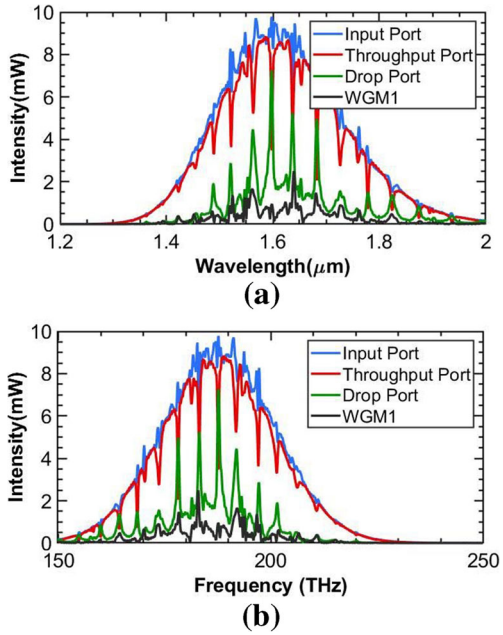

Fig. 3 The plot of the relationship between the output intensity and wavelength, frequency domain and time domains of the result in Fig. 2(a), where the Bragg wavelength results of each output are 1.59 μm, which shifted from the input wavelength at 1.55 μm. The dipole oscillation occurred at the Bragg wavelength, which shown by the two opposite side peaks along with the Bragg wavelength output. The similar signals occurred with the other dipole oscillation nodes

Where A is the amplitude of the carrier, f_i is the carrier frequency, time t_i. When bits transmit through the system, the change between the two adjacent carrier frequencies is marked as ("1") and ("0"), respectively. The bit rate (f_b) is the number of bits transmitted per second. Its unit is bits per second and T is the bit time which is the inverse of bit rate. Given$\Delta f = f_1 - f_2 = \frac{1}{\Delta T}$, which is the bit error rate (BER). In this case, $i = 1$, in which a carrier frequency used. In general, the more carrier frequency employed, the higher the bit rate obtained. The packet switching time t_i is a constant. This means that it is under the synchronous switching operation, which one FSK source is employed.

The input electric field into the system in Fig. 1 is given by an eq. (2) [20].

$$\boldsymbol{E_Z = E_0 e^{-ik_z z - \omega t}}. \tag{2}$$

Here, we define the initial electric field amplitude as $\boldsymbol{E_0}$, the input light source wavelength as λ, where the wave number in the z-axis direction is $\boldsymbol{k_z = \frac{2\pi}{\lambda}}$. The linear frequency can be defined by time t, and the angular frequency by $\omega = 2\pi\gamma$. The normalized output intensities of the system in Fig. (1) are given by [20].

$$\frac{\boldsymbol{I_{th}}}{\boldsymbol{I_{in}}} = \left[\frac{\boldsymbol{E_{th}}}{\boldsymbol{E_{in}}}\right]^2 \tag{3}$$

$$\frac{\boldsymbol{I_{drop}}}{\boldsymbol{I_{in}}} = \left[\frac{\boldsymbol{E_{drop}}}{\boldsymbol{E_{in}}}\right]^2 \tag{4}$$

The fields of the silicon microring circuit in Fig. (1) E_{th}, E_{drop}, E_{add},and E_{in} are the throughput, drop, add and input ports, respectively. The whispering gallery mode at the center microring is obtained by controlling the two side rings (two side rings act as phase modulators), from which at the resonant condition, the normalized intensity outputs at the throughput and drop ports obtained.

The silicon microring circuit comprises a center ring and two side rings, with gold grating embedded on the two side rings. The Drude model [21, 22] describes the behavior of metals and the frequency dependent dielectric function of the solid (gold) given by

$$\boldsymbol{\epsilon(\omega) = 1 - \frac{ne^2}{\epsilon_0 m\omega^2}} \tag{5}$$

The relative permittivity can be defined by ϵ_0, the electron density by n, charge by e and mass by m, where we define the angular frequency by ω . If the resonance frequency is ω_p, therefore it can be considered as the plasma frequency, where the definition of the plasma frequency is as follows,

$$\boldsymbol{\omega_p = \left[\frac{ne^2}{\epsilon_0 m}\right]^{-1/2}} \tag{6}$$

The relationship between the plasma polarization density (P) and the electric field (E) is given by an eq. (7).

$$\boldsymbol{P = -\frac{ne^2}{m\omega^2} E} \tag{7}$$

Equation 7 shows the relationship between the plasma polarization, density (P), and electric field (E), as the Bragg wavelength covers the plasma frequency. The grating corresponds to the Bragg wavelength by using the question $\boldsymbol{\lambda_B = 2n_e\Lambda}$, where we define the effective refractive index and the grating period by $\boldsymbol{n_e}$ and $\boldsymbol{\Lambda}$ respectively. The coupling power varies with respect to the grating dimensions for propagation of light within each nanograting. Kerr effect exist through the structure and it can be included in the $\boldsymbol{n = n_0 + n_2 I = n_0 + n_2 P/A_{eff}}$ equation (8), where the linear and nonlinear refractive indices can be defined by $\boldsymbol{n_0}$ and $\boldsymbol{n_2}$ respectively. Other parameters such as I, P, and $\boldsymbol{A_{eff}}$, are defined as optical intensity, optical power and effective mode area respectively. The $\boldsymbol{A_{eff}}$ varies in the range of 0.1 to 0.50 $\boldsymbol{\mu m^2}$, for the microring resonators. In this case, the Bragg wavelength of each sensor node is the same, which shifted from the original input wavelength. The self-calibration of each node of the microring circuit can be applied.

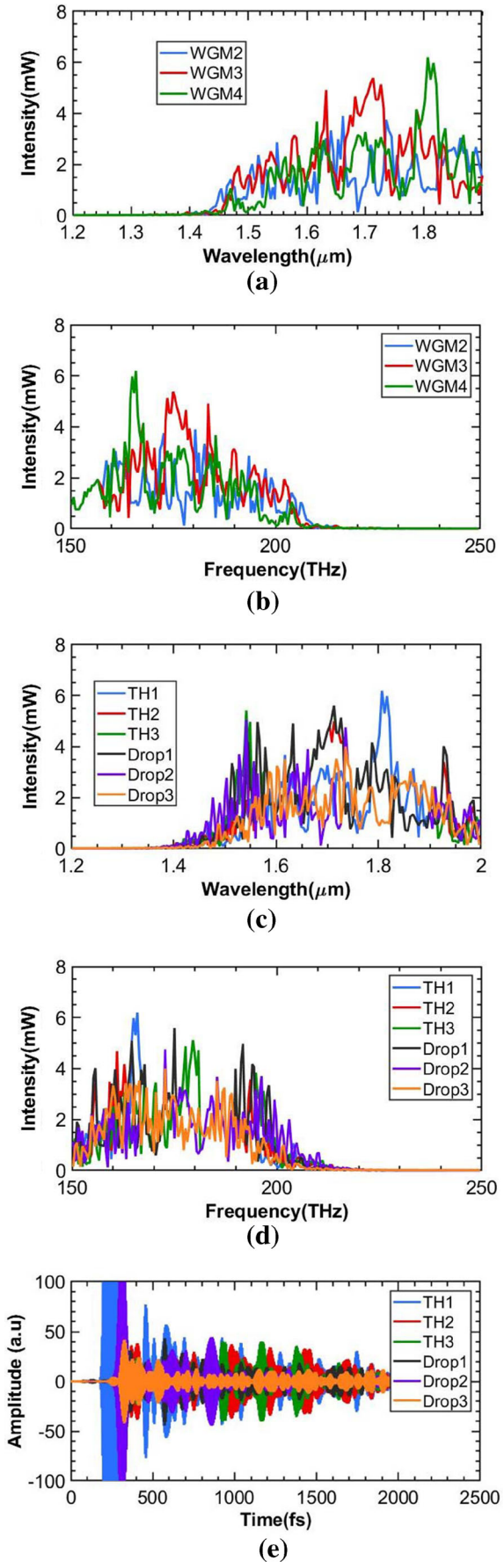

◀ **Fig. 4** Results of the MATLAB program of the results in Fig. 2(b), where (a) and (b) WGM of the three user nodes in wavelength domain and frequency domains, and (c), (d) and (e) are the through ports and drop port in time domain, wavelength domain and frequency domain, respectively

3 Results and Discussion

The proposed system uses the input light source with input wavelength of 1.55-μm as shown in Fig. 1.The 32-bit version 12.0 [23] of the Optiwave FDTD program is used for simulating the system. The grid size of the simulation is implemented automatically by the program with the number of mesh cells of 308, 55, and 353 for three axes (x, y, and z). The anisotropic perfect matched layer employed as the boundary condition with 15 layers, real tensor of 1.0 and 1.0×10^{-12} theoretical reflection coefficient. Table 1 presents the system parameters. The coupling between the light and the gold grating produces the plasmonic polaritons at the resonance condition, where the light propagations with existence of the Bragg wavelength can be formed in the rings located in the sides of the centered ring and the centered ring itself. The output ports including the thorough and drop ports guide the output signals, where the multiplexing and demultiplexing of the required information can be performed by using the other ports as add and drop ports. The FDTD is the used method to perform the computations, where particular system parameters such as the resonance wavelength can be utilized to trap the light in the proposed microring resonator structure. The power transmitted from the throughput port in Fig. 1a goes through to Fig. 1b, the three silicon microrings will resonance at a frequency where the two side rings which act as phase modulators will influence the directivity of the beam propagation due to the nonlinearity effect. Figure 2 shows the result of the WGM formed at the two side rings and center rings from Fig. 2(a). Figure 2(b) shows the WGMs formed at the three center rings. The whispering gallery mode output observes at the center wavelength, which is the Bragg wavelength of each ring center. The nonlinear effect exhibited by the two silicon microrings caused the trapped light at the center of silicon microrings. By using the resonant results, the number of round trips was 20,000. In

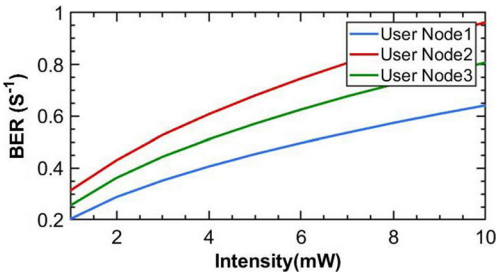

Fig. 5 The results of the MATLAB program of the results in Fig. 2(b), comparing the BER of the user nodes from Fig. 2(b) at the Bragg wavelength of each node, the BER increased with the distance and input power increased, the optimum BER of node 2 is 0.9 $bits^{-1}$

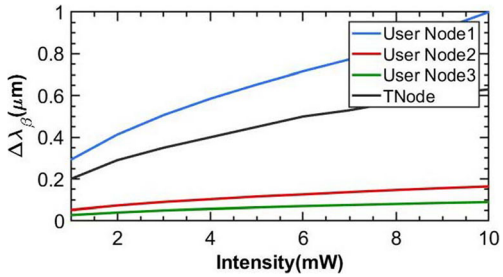

Fig. 6 The plot of change in Bragg wavelength and input power for input power 1–10 mW, where TNode is the transmitting node from Fig. 2(a) with sensor sensitivity of 0.04 μm $(mW)^{-1}$, while the user nodes 1–3 are the receiving nodes from Fig. 2(b) with sensor sensitivities of 0.15 μm $(mW)^{-1}$, 0.09 μm $(mW)^{-1}$ and 0.18 μm $(mW)^{-1}$ respectively

manipulation, the input power varied from 1 to 10 mW. The input source was the Gaussian pulse. The suitable coupling coefficient was 0.5. Fig. 3 shows the result of the relationship between the normalized intensity and the wavelength, frequency and time domains of the results in Fig. 2a, respectively. The Optiwave program used the FDTD algorithm, and the parameters extracted from the Optiwave program used in the MATLAB program to plot the WGM of the user nodes in Fig. 4. The WGM2-WGM4 signals at the distributed nodes are the distributed LiFi signals. The bit error rate is shown in Fig. 5 where the optimum BER of node 2 is 0.9 bit $^{-1}$. The change in Bragg wavelength with varying power is shown in Fig. 6 where the linear trend can be used for sensor sensitivity. Bit error rate (BER) gives the performance of a network comparing the transmitted signal through the 10 km fiber channel to the received signal at the user nodes. The result in Fig. 5 shows that the BER increased when the input power increases. The proposed system can support the dual modes of transmission, which can either apply by wireless or cable connection. The LiFi network can connect through the WGM output, which can connect by the cable or wireless. In our study, the cable transmission of LiFi considered by using the device ports; that is transmitting through the throughput port and distributed to the network distributors. Finally, the applicants can connect to the network in both LiFi and cable connections.

By using both dual transmission modes, the LiFi and cable connections can apply and have a high transmission capacity. Moreover, the multiplexing channels of information can lead to having the ultra-high transmission capacity. The electro-optic signal conversion allowed both LiFi and WiFi applicable that can have more selective detection schemes. Principally, the polariton wave oscillation induced by the gold grating coupling effect can have the dipole oscillation, which is the micro-antenna propagation and available for LiFi use. The electro-optic conversion can also have the polarization (polariton spin) and electron spin detection schemes, which allowed the quantum detection applicable [13, 14, 28]. The sensor application and 3D imaging transmission are also available by using the WGM outputs [29], which formed by the micro-conjugate mirror. Therefore, high capacity and security transmission can be obtained and used to serve the 5G technology requirement. The fiber loss used 0.1 dBkm^{-1}, wherethe input power was 10 mW.The remained margin power after 10 km distance and 3 distributed nodes are~5 mW. It is available for more distributed nodes, where the FSK bit rate increased by applying FSK multiplexing sources. The asynchronous multiplexing can also apply as in an eq. (1), where i> 1. The asynchronous multiplexing can also be applicable as shown in an eq. (1). It is available for stenographic technique [30], where the ultra-high security and capacity can achieve. The sensing signals can multiplex with the FSK and transmit to the network. The optimum sensor sensitivity of 0.18 μm $(mW)^{-1}$ is obtained from the distributed nodes. The other sensor environment can also apply at each sensing node in the distributed network.

4 Conclusion

We have proposed a microcircuit design including microring resonators for FSK generation, where the results confirm the suitability of the proposed design for the application. The research focuses on the whispering gallery mode of light as well as the nonlinear effect occurred within the system due to using the unique proposed system. As for future work, the proposed system can be utilized for many applications such as (i) LiFi and (ii) cable networks with a high system and signal processing performance. The main operation of the circuit is the transmission of data using the advantage of LiFi, where there is little loss of data in the transmission line, while the broad bandwidth obtained. The bit error rate increases with increasing input power. There is a linear trend of the change in Bragg wavelength with input power, which is available for sensor application. Moreover, the microring resonator has the nonlinearity ability to use its nonlinearity effect, which is a unique design that can have two inputs and outputs that lead suitable for various applications. The transmission bit rates of ~200 $Tbits^{-1}$ is achieved, with the BER is ~0.9 $bits^{-1}$. This design can be used for various applications, for instance, for ultra-high bit rate transmission data with LiFi, especially, for the 5G requirement, where the additional advantages are security, more reliable detection schemes and small scale system.

Acknowledgments One of the authors (Mr. **Arumona)** would like to thank the Ton Duc Thang University, Vietnam for their financial support.

References

1. Wilson SK, Dobre OA (2016) Transmission techniques for digital communications. Academic:333–367
2. Sushmaja K, Fazal N (2013) Implementation of binary shift keying techniques. IJETT 4(6):2581–2583

3. Tso-Cho C, Shin-Wei C (2008) MFSK modulation recognition using the maximum-likelihood method with noncoherent detection. J. Chin. Inst. Tech. 39:97–106
4. Harald H, Cheng C, Dominic O (2017) A guide to wireless networking by light. Prog. Quantum Electron 55:88–111
5. Praveen B, Punil N, Sravanthi M (2014) Li-fi (light fidelity): the next generation of wireless network. ICETETS 3(1):132–137
6. Shailendra Y, Pradeep M, Minakshee V, Togrikar PS (2016) Li-fi technology for data transmission through LED. IJIR 2(6):1–4
7. Shahzad H, Kamran S (2017) Li-fi technology: data transmission through visible light. Int Scholarly Sci Res Innov 11(7):923–926
8. Shayether K, Asmina SA, Fernando MJE, Sheshadari KJ, Rangari HAT, Dhishan D (2016) Li-fi: use of visible light communication to increase performance of data transmission. IJSRP 6(4):483–487
9. Sowmiya M, Visal G (2016) A study on LiFi wireless visible light communication. IJEDR 4(1):116–119
10. Sharma PK, Ryu JH, Park KY, Park JH, Park JH (2018) Li-fi based on security cloud framework for future IT environment. Hum-cent. Comput. Info. 8:1–23
11. Anurag S, Shalabh A, Asoke N (2015) Li-fi technology: data transmission through visible light. IJARCSMS 3(6):1–12
12. Punthawanunt S, Aziz MS, Phatharacorn P, Chiangga S, Ali J, Yupapin P (2018) LiFi cross-connection node model using whispering gallery mode of light in a microringresonator. Microsyst Technol 24(12):4833–4838
13. Khomyuth C, Mahdi B, Amiri IS, Youplao P, Pornsuwancharoen N, Yupapin P (2018) Electric-optic conversion circuit incorporating a fiber optic loop for light fidelity up-down link use. Microw Opt Technol Lett 61(2):526–531
14. Youplao P, Chaiwong K, Amiri IS, Punthawanunt S, Pornsuwancharoen N, Yupapin P (2019) Broadband photon squeezing control using microring embedded gold grating for LiFi-quantum link. S.N. Appl Sci 1(5):482–488
15. Noel F (2017) Frequency shift keying with LMX2571. Texas Instrument Incorp (SNAA309):1–10
16. Mahendra P (2013) Implementation of FSK modulation and demodulation using CD74HC4046A. Texas Instrument Incorporated (SLAA618):1–13
17. Todd D (2017) PSoC3 and PSoC 5LP: low-frequency FSK modulation and demodulation. Cypress:1–13
18. Hemalatha S, Imran SK, Nirupa T, Kishore YS, Chandra BC (2018) Implementation of FSK transceiver using software defined radio (SDR). IRJET 5(3):583–586
19. Wu CF (2013) Analysis, design and implementation of FSK modulate systems. ICSEM:0616–0619
20. Pornsuwancharoen N, Youplaoa P, Amiri IS, Ali J, Poznanski RR, Chaiwong K, Yupapin P (2018) On-chip polariton generation using an embedded nanogratingmicroring circuit. Results in Physics 10: 913–916
21. Robert LO et al (2012) Optical dielectric function of gold. Phys Rev B 86(235147):1–9
22. Derkachova A, Kolwas K (2007) Size dependence of multipolar plasmon resonance frequencies and damping rates in simple metal spherical nanoparticles. EurPhys J-spec top (144):93–99
23. OptiFDTD Technical Background and Tutorials (Finite Difference Time Domain) Photonics Simulation Software, Version 12.0. http://www.optiwave.com, Searched on 20th Sept, 2019
24. Suresh N, Hemalatha P, Dhanabagyam S, Prabhaharan K (2015) Study of plasmonic resonance of gold through refractive index. J Mater Sci Eng 4(1):1–3
25. Gaussorguesand G, Chomet S (1994) Infrared thermography paperback microwave and RF techniques and applications. Springer
26. Yee KS (1966) Numerical solution of initial boundary value problems involving Maxwell's equations in isotropic media. IEEE Trans Antennas Propag 14(3):302–307
27. Pornsuwancharoen N, Amiri IS, Suhailin FH, Aziz MS, Ali J, Singh G, Yupapin P (2017) Micro-current source generated by a WGM of light within a stacked silicon-graphene-au waveguide. IEEE Photon Technol Lett 29(21):1768–1771
28. Silverstone JW, Santagati R, Bonneau D, Strain MJ, Sorel M, O'Brien JL, Thompson MG (2015) Qubit entanglement between ring-resonator photon pair sources on a silicon chip. Nat Commun 6:7948
29. Phatharacorn P, Chiangga S, Yupapin P (2016) Analytical and simulation results of s triple micro whispering gallery mode probe system for 3D blood folw rate sensors. Appl Opt 55(33):9504–9513
30. Zhang X, Zhang W, Wang S (2007) Efficient double-layered steganographic embedding. Electron Lett 43(8):482–483. https://optiwave.com/. Accessed 20 May 2020